# Stereo PIV measurement of diffuser swirling flow

*Pavel* Procházka[1,*], *Václav* Uruba[1,2], *David* Štefan[3], and *Pavel* Rudolf[3]

[1]Institute of Thermomechanics, ASCR, v.v.i., Dolejškova 5, Praha 8, CR
[2]UWB, FME, Department of Power System Engineering, Universitní 8, Plzeň, CR
[3]BUT, FME, Viktor Kaplan Department of Fluid Engineering, Technická 2896/2, Brno, CR

**Abstract.** The swirling flow in a diffuser has been studied using the stereo PIV technique. The DANTEC hardware and software were used for the experiment. The water pipe flow in the diffuser inlet has been set spinning by introducing tangential jet flow. Both piping and diffuser were of circular cross-section, however diffuser casing had rectangular (square) cross-section. The plane of measurement was located perpendicular to the flow within the diffuser. The two cameras with the Scheinpflug lens mounting were used, however the angle between the lenses axes and the diffuser outer surface was far from to be perpendicular, as recommended in similar situations. This configuration has been dictated by technical conditions in the laboratory. The two-level calibration target with dots was used for the cameras calibration. The calibration covers the diffusers central region in a good quality, however regions close to the walls were not well resolved. Many combinations of axial and tangential inflow conditions have been studied. The acquisition covered about 3 seconds in real time with frequency 500 Hz. Both statistics and dynamics of the flow have been studied in details.
Results are shown for both statistical characteristics and dynamical analysis of various conditions. During experiments the air-glass-water interface was not normal to the camera viewing axis. The discussion how to solve this problem and of the bias of the calibration will be introduced.

## 1 Introduction

Recently, renewable energy sources are rapidly implemented into the power grid. However, their big disadvantage is highly fluctuating power output which is a big challenge to be compensated. Hydraulic turbines (able to operate in reversible mode) are adequately appropriate for this purpose. The compensation of power fluctuation in real time results in the demand that such turbine must work within a wide range of working regimes. These regimes far from designed one are accompanied by presence of pressure fluctuations and self-induced instabilities as a consequence of decelerated swirling flow developed in diverging section well-known as precessing helical vortex (vortex rope).

The considerable pressure fluctuation are propagated through the entire flow domain which could result in rotor blades damage [1] or even, when the frequency of pressure pulsation is equal to natural frequency (eigenfrequency) of the device [2], the destruction of the entire system. There are some possibilities to control this phenomenon. Passive methods (e.g. various fins, grooves etc.) have the same effect for all working regimes without the possibilities to turnig off their effect. The active method to reduce the unwanted flow instabilities can be for example jet injection along the machine axis from the runner crown [3].

Since this experimental investigation follows on previously conducted study of instabilities in the vicinity of the airfoil [4], the used experimental facility and processing methods are similar. To examine the swirl flow in a diverging pipe, the time-resolved stereoscopic Particle Image Velocimetry (TR-PIV) was used to measure all three velocity components in a given plane. Further analysis is conducted using FFT (Fast Fourier Transform) and mainly using well-known dynamical decomposition method POD (Proper Orthogonal Decomposition). This method was introduced by Lumley [5] in seventies to fluid mechanics and proved to be effective in study of vortex rope dynamics [6].

## 2 Experimental setup

The swirling flow in the diffuser was created by mixing of axial inflow with tangential inflow coming from the spiral casing. Various regimes were characterized by different rate of both components. Nominal flow rate is a sum of axial and tangential flow: $Q_N = Q_A + Q_T$. The Dantec hardware and software was utilized. Dynamical mode decomposition method was used.

### 2.1 Swirl generator apparatus

The swirling flow is generated by swirl generator apparatus depicted in figure 1a. It consists of plexiglass diffuser with 8° divergence angle. Measurements were conducted in closed-loop hydraulic circuit consisting of

* Corresponding author: prochap@it.cas.cz

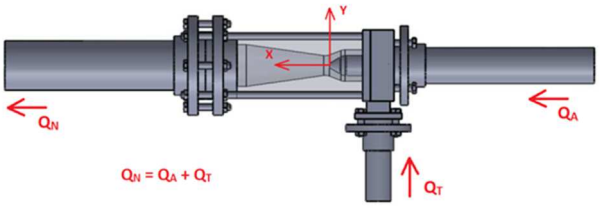


**Fig. 1a.** Design of the swirl flow generator.

centrifugal pump, stainless steel pipes, pressurized vessel and induction flow meters. While piping and diffuser were of circular cross-section the spiral casing of tangential inflow has rectangular cross-section. Swirl generator was designed as bladeless with tangential and axial intakes. Flow ratio was adjusted by valves. Such kind of design allowed sufficient control and the manufacturing costs were much lower than with rotating or stationary blades.

The flow parameters were measured by several sensors (Table 1). The flow rate was measured with two induction flowmeters (one in main pipe, one in tangential intake). Also pressure measurement points were set twice in inflow pipes, in outflow pipe and also in suction tank.

**Tab. 1.** Instrumentation.

| | **Brand** | **Specification** |
|---|---|---|
| Flow meter nominal | ELA | DN 80, PN 1,6 MPa |
| Flow meter tangential | ELA | DN 50, $Q_{max}$=20 l/s |
| Temperature sensor | PTP 55 | -5°C – 55°C |
| **Pressure sensor** | **Brand** | **Range (bar)** |
| Axial inflow | BD sensor | 0-6 |
| Tangential inflow | BD sensor | 0-6 |
| Outflow | BD sensor | 0-2,5 |
| Suction tank | BD sensor | 0-10 |

**Tab. 2.** Operating regime of cross-sectional plane measurements.

| OR | Ax. comp. (%$Q_n$) | Tan. comp. (%$Q_n$) | $Q_n$ (l/s) | Pump rev. n ($min^{-1}$) |
|---|---|---|---|---|
| 1 | 100 | 0 | 10 | 500 |
| 2 | 90 | 10 | 10 | 500 |
| 3 | 80 | 20 | 10 | 500 |
| 4 | 70 | 30 | 10 | 500 |
| 5 | 60 | 40 | 10 | 500 |
| 6 | 50 | 50 | 10 | 500 |
| 6,5 | 45 | 55 | 10 | 500 |
| 7 | 40 | 60 | 10 | 701 |
| 8 | 30 | 70 | 10 | 701 |
| 8x | 30 | 70 | 5 | 701 |
| 9x | 20 | 80 | 5 | 701 |
| 10x | 10 | 90 | 5 | 701 |
| 11x | 0 | 100 | 5 | 701 |

Totally 13 operating regimes were examined. Each regime is characterized by different rate of axial and tangential component (Table 2, 3). The nominal flow rate through the closed-loop circuit has been set twice smaller for regimes with high portion of tangential part due to technical reasons (these regimes are marked with x). Operating regimes (OR) could be adjusted from pure axial flow (OR 1) to flow where tangential component dominates (OR 11x). Spiral vortex breakdown was pronounced for flow beginning with ratio 50:50 (OR 6).

**Tab. 3.** Operating regime of longitudinal plane measurements.

| OR | Ax. comp. (%$Q_n$) | Tan. comp. (%$Q_n$) | $Q_n$ (l/s) | Pump rev. n ($min^{-1}$) |
|---|---|---|---|---|
| 1 | 100 | 0 | 10 | 500 |
| 2 | 90 | 10 | 10 | 500 |
| 3 | 80 | 20 | 10 | 500 |
| 4 | 70 | 30 | 10 | 500 |
| 5 | 60 | 40 | 10 | 500 |
| 6 | 50 | 50 | 10 | 500 |
| 6,5 | 45 | 55 | 10 | 500 |
| 7 | 40 | 60 | 10 | 600 |
| 8 | 30 | 70 | 10 | 700 |
| 8x | 30 | 70 | 5 | 700 |
| 9x | 20 | 80 | 5 | 700 |
| 10x | 10 | 90 | 5 | 700 |
| 11x | 0 | 100 | 5 | 700 |

## 2.2 PIV setup

The main goal of this project was to detect all three velocity components in distinct planes. Classical way how to perform the stereoscopic PIV calibration is to use a calibration target which should be moved across the measured plane [4]. Such kind of experiment (circular cross-sectional pipes flooded by water) did not allow using a plane dot matrix target.

Hence, the multi-level calibration targets with white dots on the black background were used (dot spacing 10mm, level distance 2mm, zero marker diameter 4,5mm and main marker diameter 3mm). One target was used to covered as large as possible measured area for longitudinal plane (target edge touched the swirl generator hub which was the origin of coordinate system – Fig. 1b) and the second one was established to calibrate cross-sectional plane (diameter was 70mm and location in downstream direction from the origin x = 84 mm).

Stereo arrangement of PIV was used. The set consisted of a laser with cylindrical optics and two cameras. The laser New Wave Pegasus Nd:YLF has double head emitting coherent light with wavelength 527 nm by maximal frequency equal to 10 kHz. The pulse energy is optimized for 1 kHz when its value is 10 mJ (corresponding power is 10 W per head). Two CMOS cameras NanoSense MKIII were used, resolution 1280 x 1024 pixels and maximal achievable acquisition frequency about 500 Hz. The memory is 4 GB. The

cameras were used with Scheinpflug lens mounting, however, the angle between lenses axes and the diffuser outer surface was far from to be perpendicular, as recommended in similar situation [7, 8]. This configuration has been dictated by technical conditions in the laboratory. As tracing particles, hollow glass spheres coated with silver were used.

The longitudinal plane oriented with diffuser axis as well as cross-sectional plane were in the centre of investigation. The first one covers the flow region from the top of the hub to x = 140 mm downstream. The calibration model (pinhole model) was applied on picture of multi-level calibration target. The reprojection error was set approximately 1 pixel which is still satisfying according recommendation. Finally, we got the velocity vector maps with 129 x 110 vectors (up to 12% of substituted vectors) corresponding to space resolution approx. 1 mm.

The second measured plane was established to cover as large cross-section as possible. The enormous optical distortion made the calibration very difficult. Although the Direct Linear Transform is unable to model any non-linear distortion, just this calibration model was able to calibrate stereoscopic arrangement. However, the reprojection error was far from recommended values, so the cross-sectional plane values should be treated as qualitative ones. The final velocity vector map has 104 x 64 vectors (up to 15% of substituted vectors).

The acquisition frequency was set to 100 Hz during 10 sec of measurement and to 500 Hz (3 sec) to evaluate the statistical quantities and for dynamical analysis, respectively.

**Fig. 1b.** Used multi-level PIV target.

### 2.3 POD

The flow with vortex rope inside the diffuser is typically complex field to which it is possible to apply Proper Orthogonal Decomposition (POD). POD applied on PIV data is a powerful method of for dynamic flow features analysis. It is a good tool to interpret snapshots in order to distinguish between coherent flow patterns and random flow variations. POD analysis is very often applied on spatiotemporal 2D data; we apply it to all three components of velocity vector in our case. Most researchers apply this analysis to fluctuation part of scalar quantity (vel. components, pressure, etc.) [9]. Result is a set of orthogonal modes according to the relative kinetic energy content (mode No. zero is actually mean flow). Low-order modes have high content of energy and their topos is created by large/coherent structures while high-order modes have the energy content less than approx. 0,5% and their topos contain very often only turbulent noise or measurement bias. Further information about decomposition methods can be found in work of Uruba [10].

## 3 Results

The presented vector field will be plotted in dimensional form. Coordinate system origin is located at the end of the hub. Black vectors represent the velocity projected onto the plane of measurement. The color represents other scalar value (third vel. component, velocity variations etc.). The swirl motion can be detected in cross-sectional planes by black vectors orientation and also by comparison of positive and negative out-of-plane velocities in longitudinal plane. Note, that the direction of the vectors is not meaningful in the case of POD modes as the calculation comes from the vel. fluctuation. The vorticity distribution is used here to detect vortices (no shear layers are expected). Positive vorticity identifies the counter-clockwise rotation (red color).

### 3.1 Mean flow field

The flow inside the diffuser seems to be stable for time-averaged quantities. No secondary vortices and no flow separation close to the walls are present. The flow of regime No. 2 is characterized by flow deceleration along streamwise coordinate as the flow cross-section becomes wider. Highest velocities are located just behind the hub where the diffuser diameter is 50 mm. Mean velocity value is higher than 5 m/s in this region. Flow is spread across the diffuser almost homogeneously with boundary layer close the walls (see Fig. 3a). No significant swirl motion is detectable in the whole area (Fig. 2a). The regime No. 8, which is characterized by 70% of tangential component, is characterized by the existence of considerable helical vortex structures (Fig. 2b, 3c). The structure rotates in counterclockwise sense which is given by the connection of the tangential intake to the swirl generator. The highest velocities were detected in annular region between boundary layers and the diffuser axis. The area of backflow is getting more important with increasing of tangential component. There is a tiny backflow just in the diffuser centre for regime No. 5 (depicted in Fig. 3b). On the other hand, more significant backflow region is visible in figure 3c, where regime No. 8 is captured. Since the backflow area is increasing with tangential flow rate component, the positive streamwise vel. components are also increasing and are located more close to the walls (well visible in longitudinal planes). The integration of streamwise vel. component will lead to equal nominal flow rate for all regimes – 10 or 5 l/s according to table 2, 3.

The distribution of turbulent kinetic energy (TKE) which is given by equation

$$TKE = \frac{1}{2}\{\overline{(u')^2} + \overline{(v')^2} + \overline{(w')^2}\} \qquad (1)$$

represents the fluctuation activity of the flow. The fluctuation is getting greater for higher OR and the most significant region is located in the diffuser axis at x = {20-40} mm. Just in this area, the merging of annular stream deflected by the hub is responsible for such high vales of TKE (Fig. 2c). Velocity variations are smaller further downstream as we can see in figure 3d (84 mm downstream the hub). There the fluctuation is significant mainly in annular cross-section.

Based on time-averaged PIV data, the flow topology is strictly dependent on the flow rate through the tangential branch. There is no dependency on the nominal flow rate at all (there is no difference between regime No. 8 and No. 8x).

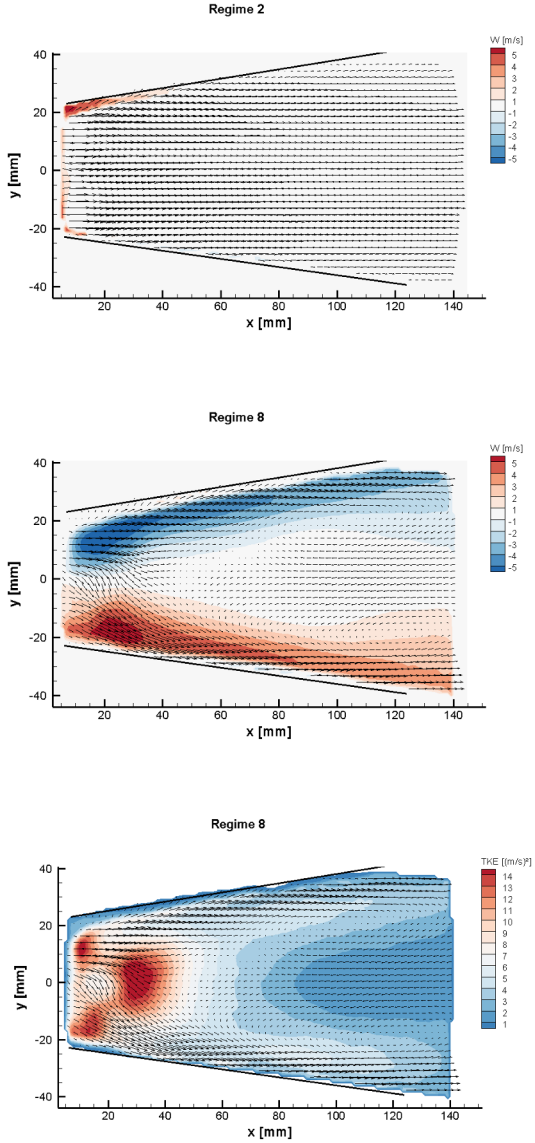


**Fig. 2a, b, c.** Longitudinal planes, distributions of out-of-plane velocities (a, b) and turbulent kinetic energy (c).

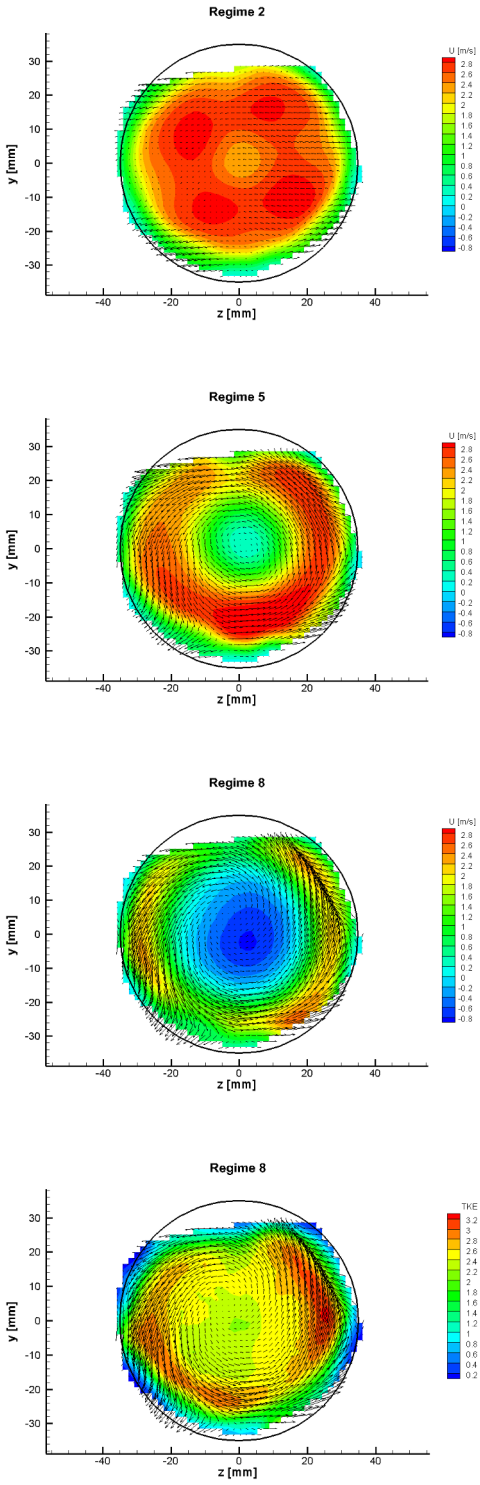


**Fig. 3a, b, c, d.** Cross-sectional planes, distribution of streamwise velocity component (a, b, c) and TKE (d).

### 3.2 Instantaneous flow field

The snapshots (Fig. 4a, b) have highly turbulent character of the flow patterns. The main helical vortex pattern is overshadowed by smaller secondary vortices located close to the diffuser walls. The flow field is completely chaotic and differs for each time step. There

is an indication of rotating vortex approaching toward the upper wall and deflected by an angle approx. 30°.

The information from these snaps will be applied for POD analysis and for spectrograms. The determination of Strouhal number will be carried out only for longitudinal plane due to more precise calibration.

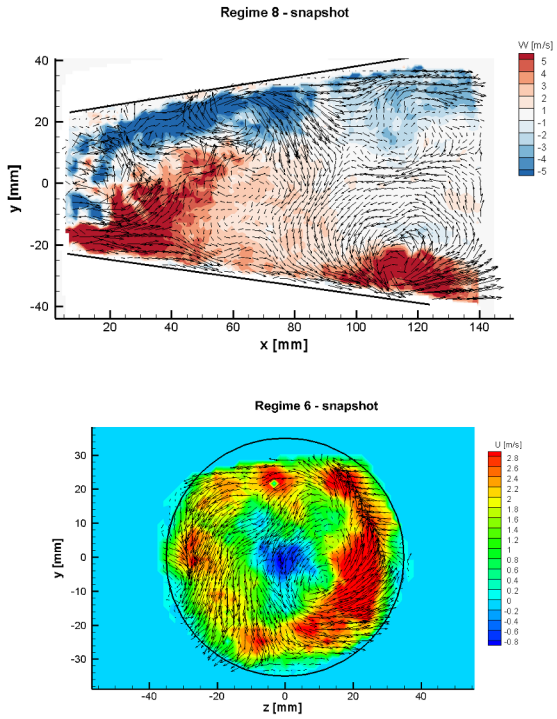


**Fig. 4a, b.** Instantaneous flow fields, longitudinal (a) and cross-sectional (b) planes.

### 3.3 Dynamical aspects

The decomposition using POD was applied on fluctuation part of all three vel. components calculated by subtraction of mean part from all snapshots. After that the temporal correlation matrix is formed, the main principle is solving the eigenvalue problem [10]. The set of POD modes is a product of this analysis. The modes are ordered according to relative energy content. Generally it can be said, that POD is not able to associate distinct frequency value to one individual POD mode (this problem solves another method). Nevertheless, an assumption for the frequency can be done very often; except the case when POD mode is associated with significant broadband.

There is a trend of kinetic energy content for longitudinal plane and for cross-sectional plane in figure 5a and 5b, respectively. The red line is plotted for energy of the very first POD mode in dependency on various OR. The blue line is actually the energy sum of first ten modes also in dependency on tangential fraction of the flow rate. The mode with highest energy fraction starts occur for regime No. 8 and higher. The first POD mode has almost 20% of relative kinetic energy. We can also see from these graphs that the sum of ten modes contains almost 50% of energy for longitudinal plane and even more than one half for cross-sectional plane. This tendency occurs from $Q_T > 50\%$. It is clear that the most energetic dominant structures stop growing for flow regime having tangential fraction of mass flow rate higher that 70%.

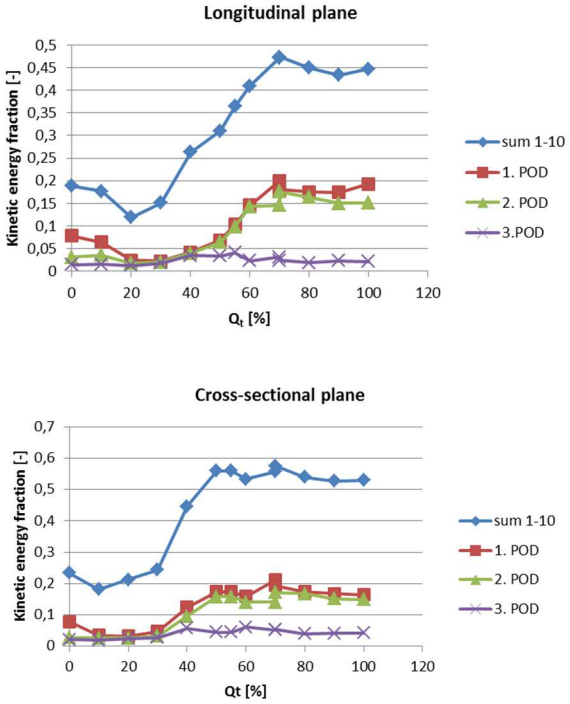


**Fig. 5a,b.** Kinetic energy fraction of low-order modes for both planes of measurement in dependency on tangential flow rate.

Regime No. 6 (rate 50-50) was chosen as an appropriate representative case of the mode topology (topos). Figure 6a is depicted for the very first mode. It is characterized by two pairs of counter-rotating vortices near the wall. Another two much smaller pairs can be seen near the diffuser throat where they are created. The associated frequency was estimated as approx. 29 Hz. Second mode (not plotted) is very similar, its topos is phase-shifted and has the same frequency. Mode No. 3 is plotted in figure 6b. This one is associated with higher frequency (30 Hz) and contains less energy (Fig. 5a). The topos is again composed from two pairs of counter-rotating vortices, however, now, they are oriented in perpendicular sense. The vortices are located very close to the throat. Some modes with energy less than 1% are plotted further; they are high-order modes containing smaller structures mainly responsible for chaotic behaviour of the flow.

Yet another two examples of modes are plotted for cross-sectional plane in figure 7. The topos of second mode is created from two big vortices filling the whole diameter. There is a huge diagonal flow between the vortex cores. The third mode consists of four vortices situated symmetrically with a singular point in the middle.

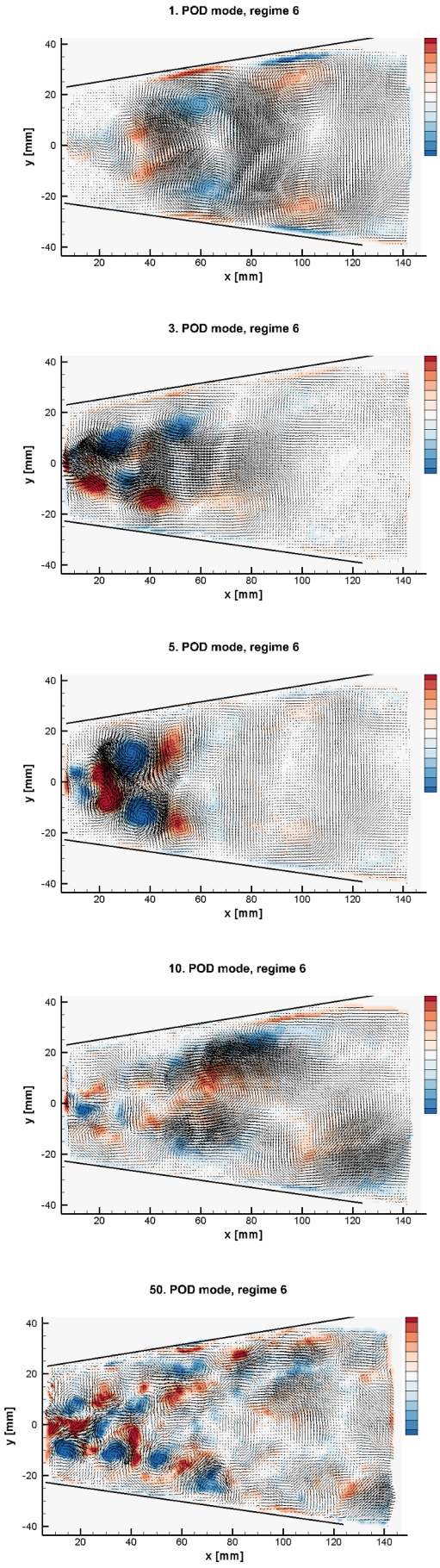


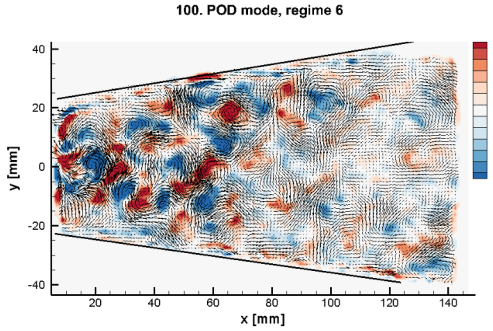


**Fig. 6a, b, c, d, e, f.** POD modes for regime No. 6, 1st (a), 3rd (b), 5th (c), 10th (d), 50th (e) and 100th (f), vorticity.

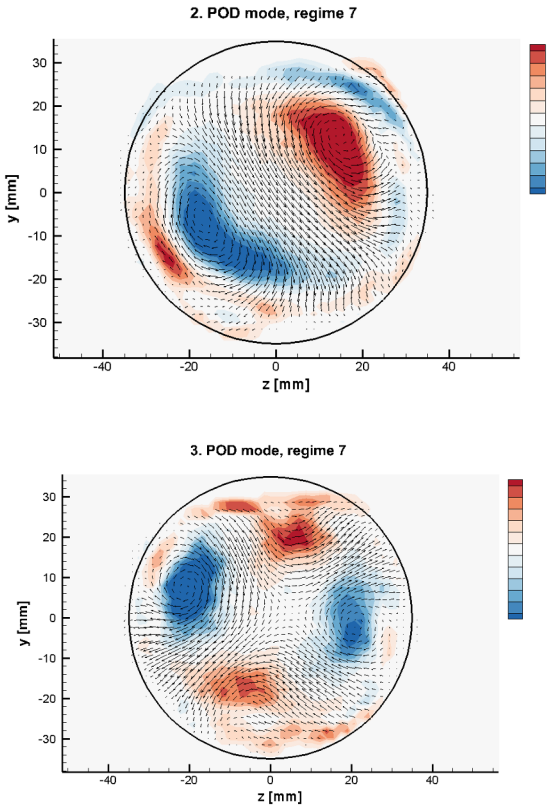


**Fig. 7a, b.** POD modes for regime No. 7, cross-sectional plane, 2nd (a) and 3rd (b), vorticity distribution.

### 3.4 Frequency analysis

The dominant frequencies occurring in arbitrary point of the flow field were investigated using FFT analysis. Only data for longitudinal plane was used. An estimation of power spectral density was conducted and the dominant frequency was found. This frequency was used to determine Strouhal number

$$Sh = \frac{f D_{ref}}{v_{ref}}, \qquad (2)$$

where $D_{ref}$ is the diameter of throat (50 mm). Referent velocity was set according to

$$v_{ref} = \frac{4Q_N}{\pi D_{ref}^2}. \qquad (3)$$

The dominant frequency of OR No. 6 was determined as 29 Hz which is exactly the same value as the associated frequency of POD mode No. 1 and 2. The last figure 8 is plotted here to show the dependency of Strouhal number on increasing fraction of tangential flow rate. The regime No. 8 and 8x were characterized by twice as different frequency value; Sh number was identical.

It was shown that Strouhal number almost linearly depends on the flow rate, which is in an agreement with findings of other authors.

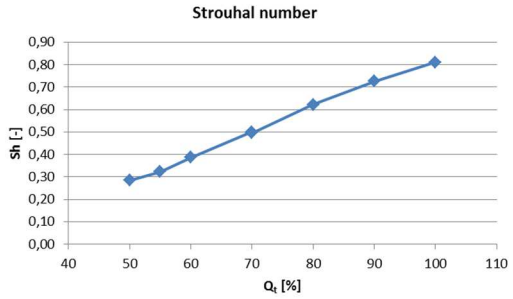


**Fig. 8.** Strouhal number dependency on used tangential fraction of the mass flow rate.

## 4 Conclusions

The stereoscopic TR-PIV measurement was conducted inside the model of swirl flow apparatus. The optical access to the measurement planes was very challenging due to complex shape of the model. The only way was to use two-level calibration target. Various calibration models were utilized to get best calibration reprojection errors. The resultant vector maps were under investigation to describe the mean flow topology and mainly dynamical flow structures and associated frequencies.

A central helical swirling vortex was detected from time-averaged flow field and snapshots. The potency of this structure is directly proportional to applied rate $Q_T$ to $Q_A$. The region with highest fluctuation activity is right behind the hub. There is no flow separation near the walls.

The spatiotemporal information in the form of POD modes was presented here for different swirling flow generated under several regimes. OR No. 8 and higher ($Q_T$ > 60%) suppresses higher POD modes as the kinetic energy of the first two modes is rapidly increasing. Next studies will be devoted to more advanced method (OPD) to uncover all frequency set present in such kind of flow.

This work was supported by the Grant Agency of the Czech Republic, project No. 17-01088S.

## References

1. D. Frunzaverde, S. Muntean, G. Marginean, V. Campian, L. Marsavina, R. Terzi, V. Serban, Failure Analysis of a Francis Turbine Runner, IOP Conf. Ser.: Earth Environ. Sci., **12**(1), 2010, p. 012115.
2. P. Dörfler, M. Sick, A. Coutu, Flow-Induced Pulsation and Vibration in Hydraulic Machinery, Springer-Verlag 2013, London.
3. D. Štefan, P. Rudolf, S. Muntean, R. Susan-Resiga, Proper Orthogonal Decomposition of Self-Induces Instabilities in Decelerated Swirling Flows and their Mitigation through Axial Water Injection, Journal of Fluids Engineering, Vol. **139**, 2017, 081101-1.
4. P. Procházka, V. Uruba, V. Skála, On the 3D Structure of the Flow-Field in the Vicinity of Inclined Plate, Journal of Physics: Conference Series, Vol. **1101**, 2018.
5. J. L. Lumley, Stochastics Tool in Turbulence, Academic Press, 1970, New York.
6. P. Rudolf, D. Štefan, Decomposition of the Swirling Flow Field Downstream of Francis Turbine runner, IOP Conf. Ser.: Earth Environ. Sci., **15**(6), 2012, 062008.
7. C. Tropea, A. L. Yarin, J. F. Foss, Handbook of Experimental Fluid Mechanics, Springer, 2007.
8. M. Raffel, C. E. Willert, S. T. Wereley, J. Kompenhans, Particle Image Velocimetry. A practical guide, Springer, 1998.
9. K. E. Meyer, J. M. Pedersen, O. Őzcan, A Turbulent Jet in Cross-flow Analysed with Proper Orthogonal Decomposition, J. Fluid Mech, **583**, 2007, pp. 199-227.
10. V. Uruba, Decomposition Methods in Turbulent Research, EPJ Web of Conference, **25**, 2012, 01095.